Geochemical characteristics of the slip zones of a landslide in granitic saprolite, Hong Kong: implications for their development and microenvironments

B.-P. Wen · N.S. Duzgoren-Aydin · A. Aydin

Abstract Geochemical investigations of the slip zones of a landslide in granitic saprolite revealed that they have signatures distinct from their host materials. These distinctions include stronger Si depletion, higher Al enrichment, greater LOI, significant fixations of Mn, Ba and Ce, stronger negative Eu anomalies, and greater accumulations of other rare earth elements (REE). Altogether, these geochemical characteristics indicate that: (a) the slip zones have greater abundance of clays, consistent with field and microscopic observations; (b) concentration of clay size particles within the slip zones may have been from downward leaching and deposition, and lateral transportation of Al-Si solutions and colloids through pores and fractures within the saprolite; and (c) there were prevailing oxidation and poor drainage, and occasional reduction conditions within the slip zones. It was concluded that geochemical analyses could be effective in gathering clues for understanding the development and nature of slip zones in landslide investigations.

Keywords Geochemistry · Slip zone · Saprolite · Hong Kong

Received: 27 April 2004 / Accepted: 19 July 2004
Published online: 15 October 2004

B.-P. Wen
Department of Hydraulic Engineering, Tsinghua University, Beijing 100084, China

N.S. Duzgoren-Aydin · A. Aydin (✉)
Department of Earth Sciences, The University of Hong Kong, Pokfulam Road, Hong Kong SAR, China
E-mail: aaydin@hku.hk
Tel.: +852-2241-5474
Fax: +852-2517-6912

Introduction

Slip zones along which landslides occur often have lower intrinsic resistance to shear. It has been well documented that slip zones of landslides most commonly develop along pre-existing weak zones dipping out of slopes, particularly if sub-horizontal (Hutchinson 1988; Cruden and Varnes 1996; Dikau and others 1996). Hence, locating and identifying such zones are vital for predicting and controlling landslides. The formation and evolution of pre-existing weak zones is a complex geological process involving chemical and mineralogical alterations within soils or rocks, particularly in tropical regions, as in Hong Kong, where weathering is dominantly chemical. Thus the weak zones should have chemical characteristics distinct from their host materials. These chemical characteristics may serve as indicators of the origin of the weak zones and their microenvironments. The pre-existing weak zones prone to slip zones of landslides are often distinguished from their host materials by greater abundance of clay size particles, distinct types of clay minerals and lower shear strength, as well as distinct physical properties, e.g., higher moisture content and poorer permeability (Skempton and Petley 1967; Kenny 1977; Anson and Hawkins 1999; Koor and others 2000). Compared with numerous studies on their mechanical properties, geochemical characterization of slip zones has been very limited in the literature. Recently, Mashana and others (1993), Anson and Hawkins (1999), Shuzui (2001) and Hürlimann and others (2001) showed that slip zones have chemical characteristics distinct from their host materials, and that these characteristics are closely correlated with physical and mechanical properties. Zheng and others (2002) found that the slip zones of four landslides in Japan contain more ferrous Fe than the sliding debris and bedrock, suggesting that the slip zones formed under stronger reduction conditions. Results are presented of a comprehensive geochemical characterization study of the slip zones of a landslide in granitic saprolite in Hong Kong. This study is aimed at exploring the potential of geochemical approach in understanding origin and microenvironmental conditions of the slip zones. A list of abbreviations frequently used in this paper is given in the appendix.

 DOI 10.1007/s00254-004-1145-6

Study site and samples

Site description

Hong Kong is characterized by a mountainous terrain and a sub-tropical humid climate with an annual average temperature of 23 °C and precipitation of 2,225 mm (Brand 1995). Principle rock types in Hong Kong are granite and acid volcanic rocks, which cover about 85% area of Hong Kong (Fletcher and others 1997). Intense chemical decomposition of bedrock produced a weak, soil-like mantle over the mountainous terrain, which is susceptible to landslides. Depth of weathering in highly fractured granite often reaches 60 m.

The landslide investigated in this paper is on the slope behind the Shek Kip Mei estate, southeastern Kowloon, Hong Kong (Fig. 1). The slope is underlain by medium-grained granite of Jurassic to Cretaceous age. The granite is intensively weathered to form a highly heterogeneous profile, showing significant zonal variations in thickness and color. At the site, highly decomposed granite (HDG) and moderately decomposed granite (MDG) forms two very thin horizons in the profile, which are laterally discontinuous at some locations, particularly near the slope toe where slightly decomposed (SDG)-to-fresh granite is locally exposed.

The landslide took place after four days of heavy rainfall at the end of August 1999. It was found that the landslide was the partial reactivation of an old landslide characterized by a large relict scar. It was developed within the saprolitic horizon made up of completely decomposed granite (CDG) and frequent corestones of slightly-to-moderately decomposed granite. The landslide area was divided into two zones, namely northern and southern distressed zones (NDZ and SDZ) based on their distinct deformation features (FMSW 2000) (Fig. 1). Slip zones of the landslide were disclosed near the toe of the slope at a number of trial pits and trenches (Fig. 1). It was observed that the slip zones of the two distressed zones are also distinct in terms of their field characteristics.

The slip zone at NDZ was composed of two distinct sections. The northern section was developed through CDG, and distinguished from the surroundings by its much wetter, softer and more clayey nature, and darker brown color (Fig. 2), while the central to southern section was along a pre-existing clay seam within CDG, and characterized by its very clayey nature and generally dark gray, locally mottled dark gray and white color (Fig. 3). The clay seam is believed to be developed along a relict sheeting joint (FMSW 2000). The slip zone at the northern section, i.e. the clayey CDG, was generally 15–25 mm thick and dipping at 7–11° out of the slope. The slip zone at the central to southern section, i.e. the clay seam, was about 15–20 mm thick, dipping at 7–10° out of the slope, generally planar and locally undulating. Scanning electron microscope (SEM) images showed that the slip zones in both sections were strongly reworked in which particles were oriented to a certain extent, an evidence of the occurrence of shear deformation (Wen and Aydin 2003, 2004).

The slip zone at SDZ formed along a pre-existing clayey seam within CDG, which was also developed along a relict

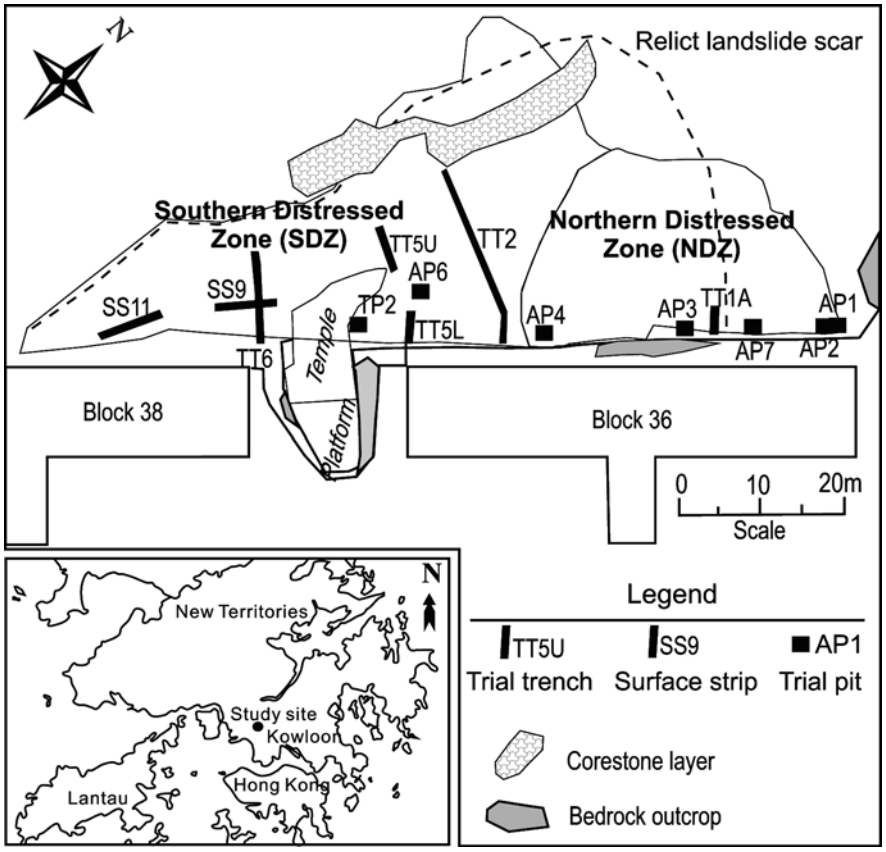

Fig. 1
Plan and location of Shek Kip Mei landslide

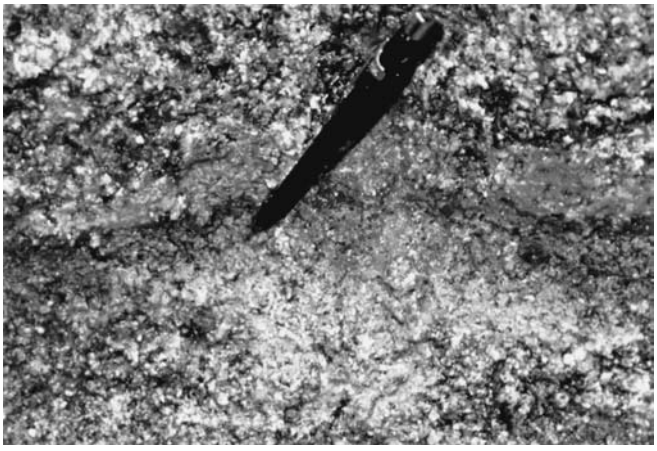

Fig. 2
Slip zone at trial pit AP7

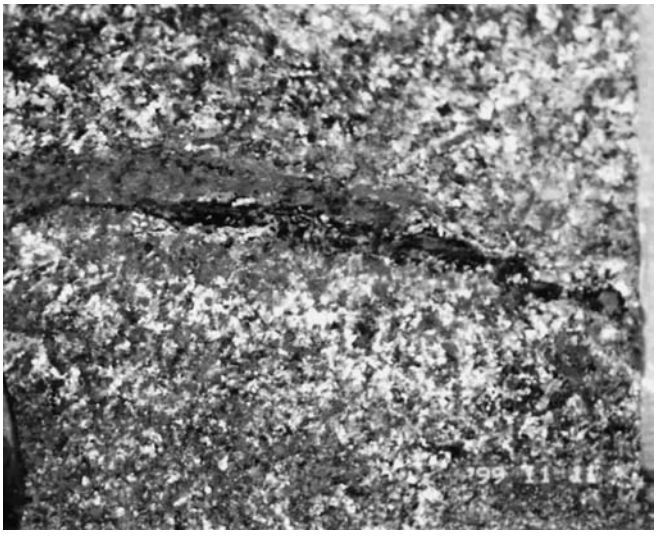

Fig. 3
Slip zone at trial trench TT1A

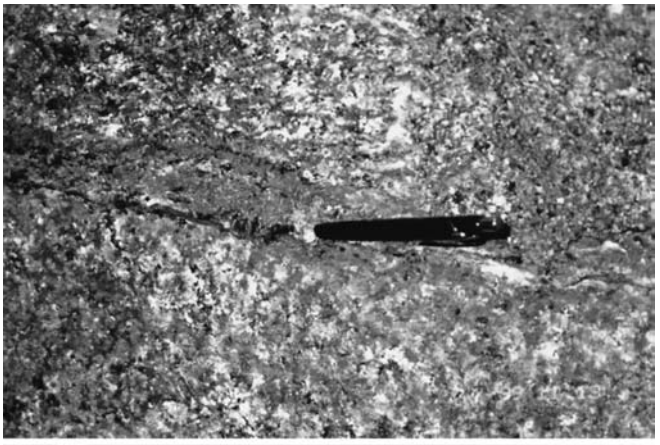

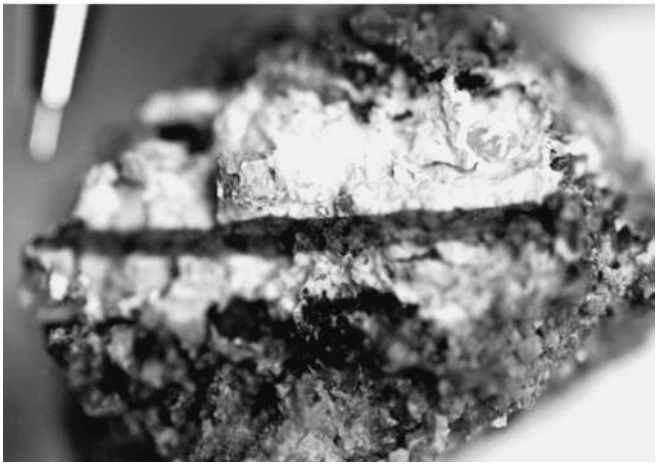

Fig. 4
Slip zone at trial trench TT2

sheeting joint (FMSW 2000). Unlike that of NDZ, the clay seam at SDZ is much thinner (3.5–12 mm), more clayey, and dipping at 6–10°, is not very wet and soft. It comprises two distinct sub-seams: a dark gray seam and laterally discontinuous two white seams (Fig. 4). The dark gray seam (DGS) (0.05–2 mm) is generally sandwiched, or occasionally overlain/underlain by the white clay seams (WS). Well-developed slickensides were observed on the surface of DGS. SEM observations illustrate that DGS has obviously experienced deformation marked by well-developed particle orientations, while no sign of deformation, or locally very slight deformation was observed within WS, evidenced by its generally intact, locally slightly reworked structure (Wen and Aydin 2003, 2004), indicating that the actual slip zone was largely confined to DGS.

Post landslide ground investigation indicated two distinct groundwater regimes within the slope: the upper (or perched) regime above the boundary between horizons dominantly of completely-to-highly and moderately-to-slightly decomposed granites, and the lower (or basal) regime not far below this boundary. The former is controlled by infiltration of surface rainwater, while the latter is a part of the regional groundwater system (FMSW 2000). Immediately after the landslide, noticeable seepage was observed at the toe of the slope, suggesting a significant rise in the upper groundwater table prior to the landslide. The slip zones were found to be within the upper regime. Extensive subvertical relict joints within the granitic saprolite facilitated interconnection of the two regimes, particularly during seasonal rise in the lower groundwater level.

Sampling

Geochemical characteristics of three profiles sampled near the toe of the slope are presented: two profiles across the slip zone of NDZ at trial pit AP7 and trial trench TT1A, and one profile across the slip zone of SDZ at trial trench TT2 (Fig. 1). At AP7, CDG-HDG was 20 cm below the slip zone and about 20–30 cm thick, overlying MDG-SDG. At TT1A and TT2, HDG and MDG were absent, as CDG was directly underlain by MDG-SDG. A total of 24 bulk samples were collected from the three profiles at 10–50 cm intervals according to color differences. Of these samples, 4 were from AP7, 13 from TT1A and 7 from TT2. As the

upper parts of trial pit/trenches were not accessible due to bracing bars, sample collection was conducted at 0.8 to 3.0 m below the ground surface. In addition, two samples from the clay seam of SDZ at the trial pit AP6 and surface strip SS9, and one sample of the fresh granite from a nearby outcrop were also analyzed. DGS and WS within the clay seam at SDZ were carefully split into sub-samples, and analyzed separately. Furthermore, undisturbed samples of the slip zones and their immediately underlying and overlying CDG were also collected.

Fresh granite at this site is mainly composed of anhedral to subhedral quartz (35–40%), subhedral to euhedral K-feldspar (35–40%), plagioclase (15–20%) and a minor amount of biotite (5%). CDG hosting the slip zones is mainly composed of highly to completely decomposed K-feldspar, completely decomposed plagioclase and biotite, as well as highly fractured quartz, clay minerals and secondary opaque oxides. Compared with CDG, the clay seam is dominated by clay minerals with minor residual primary minerals (<5%). Within the clay seam at SDZ, DGS, i.e. the slip zone, generally contains less residual primary minerals than WS. With systematical XRD analyses, Wen (2002) showed that halloysite, kaolinite and illite are prevalent types of clay minerals (halloysite >kaolinite >illite) within the slip zones and their host CDG (Table 1). In places, a trace amount (<2%) of interstratified illite-smectite was detected. Prominently, abundance of kaolinite within the slip zones is greater than in their host materials. Particle size analyses also confirmed that the slip zones contain much higher clay content than in the host materials (Table 1).

Analytical techniques

Geochemical characteristics of the slip zones and their host materials were determined by X-ray fluorescence spectrometry (XRF), inductively coupled plasma-mass spectrometry (ICP-MS), and energy dispersive X-ray spectrometry (EDS).

XRF technique was employed to determine the relative abundance of major oxides in the samples. Although Ti and Mn occur as minor elements in granite, the term 'major elements' in this study include Ti and Mn, in addition to Si, Al, Fe, Mg, Ca, K, Na and P. Glass beads made from the powdered representative samples and fused with Li4B4O7 and LiBr were used for major element analysis. XRF analysis was carried out using a PW2400 X-ray spectrometer.

Concentration of selected trace elements (Rb, Ba, Sc, Sr, Y, Pb, Th and U) and REE were determined using a VG Element PlasmaQuad 3 ICP-MS. The samples for ICP-MS analysis were prepared by dissolving powders of representative samples in HF/HNO_3 solution.

To explore the distribution of prevalent chemical elements within the slip zones and their host materials, microanalyses of chemical compositions were carried out using an energy dispersive X-ray spectrometer attached with a Cambridge Stereoscan 360 scanning electron microscope.

Table 1
Clay content and clay minerals within the slip zones and their host materials

Sample location	Depth (m)	Sample label	Clay (<2 mm) (%)	Clay mineral			
				Kaolinite (%)	Haollysite (%)	Ilite (%)	Interstratified illite-smectite
AP7	0.70	CDG1/AP7	3.84	9.00	80.00	11.00	+
	0.90	SZ/AP7	5.01	18.00	76.00	6.00	+
	1.05	CDG2/AP7	1.57	6.00	88.00	6.00	+
	1.10	CDG-HDG/AP7	1.21	6.00	87.00	7.00	+
TT1A	1.10	CDG2/TT1A	0.32	11.00	84.00	15.00	+
	1.20	CDG3/TT1A	0.91	8.00	89.00	3.00	+
	1.30	CDG4/TT1A	0.53	12.00	76.00	12.00	+
	1.80	CDG5/TT1A	1.17	7.00	89.00	4.00	+
	1.90	CDG6/TT1A	0.55	4.00	85.00	11.00	+
	2.00	CDG7/TT1A	1.18	10.00	83.00	7.00	+
	2.20	CDG8/TT1A	1.28	4.00	96.00	0.00	+
	2.30	CDG9/TT1A	5.92	7.00	91.00	2.00	+
	2.40	CDG10/TT1A	2.21	8.00	88.00	4.00	+
	2.50	CDG11/TT1A	4.69	5.00	93.00	0.00	+
	2.60	SZ/TT1A	10.61	14.00	84.00	2.00	+
	2.70	CDG12/TT1A	1.34	1.00	93.00	6.00	+
TT2	3.20	CDG1/TT2	3.37	19.00	77.00	4.00	+
	3.50	CDG2/TT2	6.40	10.00	86.00	4.00	+
	4.00	CDG3/TT2	5.12	10.00	86.00	4.00	+
	4.20	CDG4/TT2	4.43	8.00	90.00	2.00	+
	4.30	WS/TT2	25.0	27.00	71.00	2.00	−
	4.30	DGS/TT2	31.0	54.00	40.00	6.00	−
	4.40	CDG5/TT2	2.85	7.00	89.00	4.00	+
AP6	2.10	WS/AP6	22.0	16.00	80.00	4.00	+
	2.10	DGS/AP6	21.0	42.00	42.00	16.00	+
SS9		WS/SS9	25.0	7.00	86.00	7.00	+
		DGS/SS9	24.0	25.00	66.00	9.00	+

Note that "+" and "−" indicate if trace amount of interstratified illite-smectite is identified or not. *SZ* Slip Zone

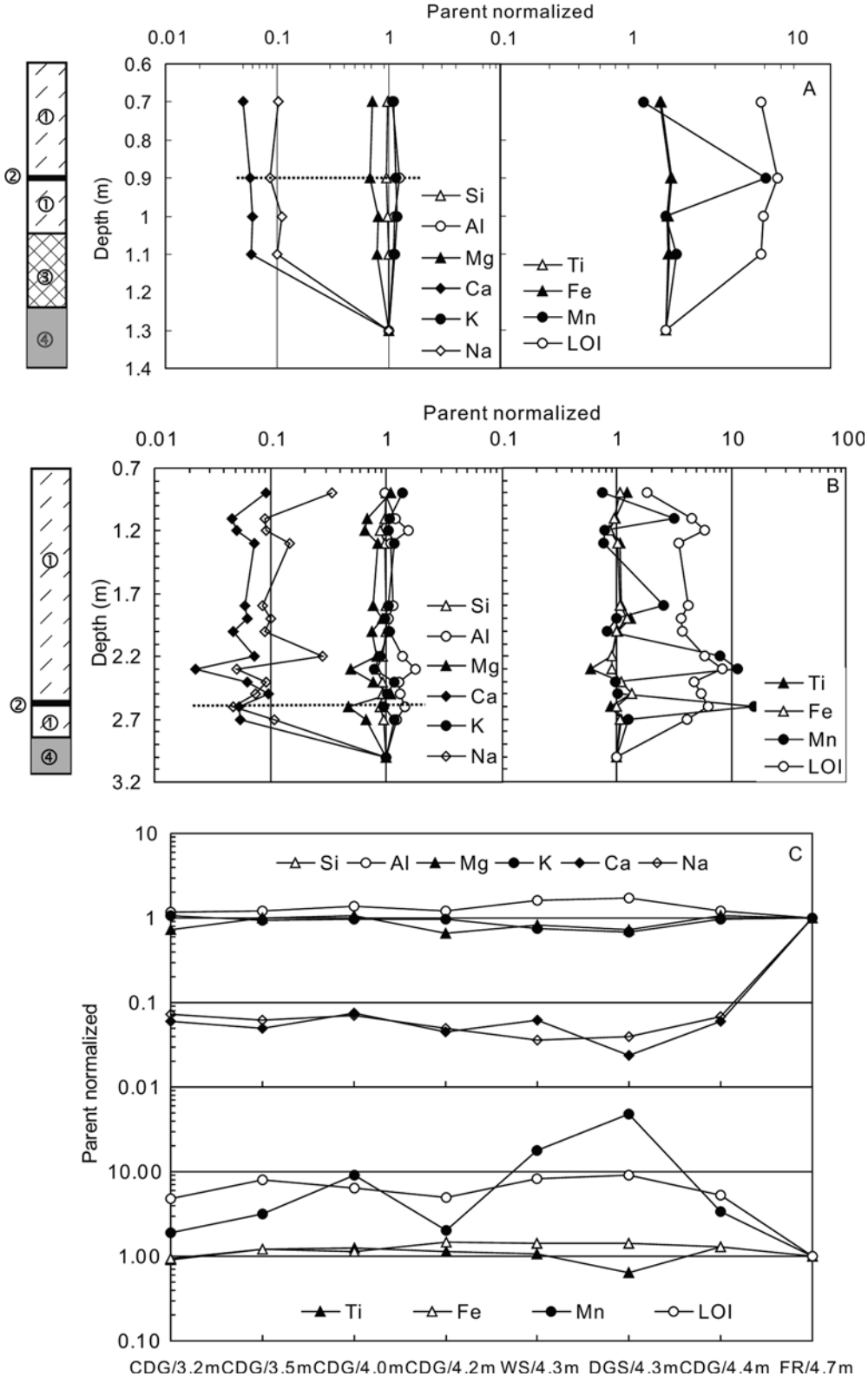

Fig. 5
Variations of major element concentrations along profiles at AP7 (A), TT1A (B), TT2(C). (①-CDG; ②-Slip zone; ③-CDG-HDG; ④-Fresh rock.)

With this technique, elements on the sample surface (ca. 1 μm deep) of an individual spot (ca. 1 μm^2) or a small area were measured semi-quantitatively based on the intensities of their X-ray spectrum. In this study, individual spot X-ray spectrum measurement and selected area X-ray element mapping were conducted. EDS analysis was carried out on the carbon coated thin sections of undisturbed samples. The thin sections were prepared from resin-impregnated samples.

Data evaluation in this study is based on three assumptions: (a) the system is open; (b) a fresh sample of the parent rock can be taken as a reference; and (c) no element is immobile (Nesbitt 1979; Middelburg and others 1988; Dequincey and others 2002; Duzgoren-Aydin and others

2002a). Therefore, concentrations of elements were normalized with reference to the fresh parent rock. When the normalized value is greater than 1, it implies that the element has been enriched or fixated. Otherwise, if the normalized value is less than 1, it indicates that the element has been depleted or mobilized. In addition, REE concentrations are also chondrite-normalized using the chondrite REE values. The normalized data along the profiles at AP7 and TT1A were plotted against depth, while those along the profile at TT2 were shown without reference to the actual sequence of WS and DGS, as only one of the two WS hosting DGS was analyzed, and WS and DGS are too thin (generally <10 mm) to be plotted in scale.

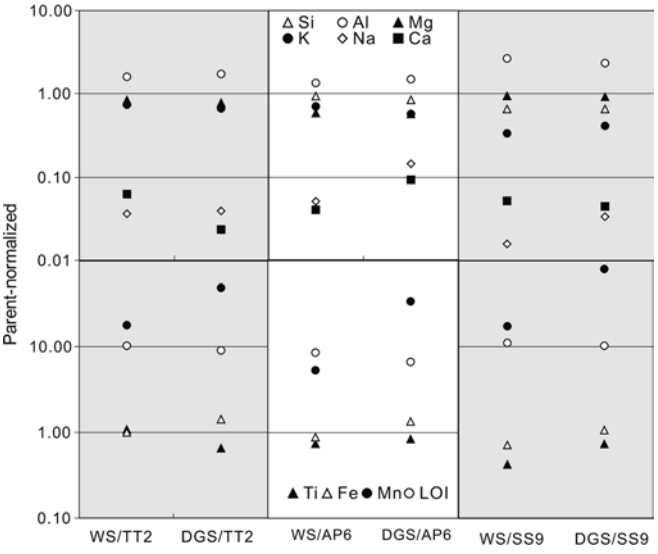

Fig. 6
Variations of major element concentrations along the clay seam at SDZ

Results

Distributions of major elements

Relative to the fresh granite, Fig. 5A–C consistently illustrate that within the slip zones and their host CDG, there are: (a) substantial depletion of Ca and Na, ubiquitous depletion of Mg, and slight depletion of Si (Ca>Na>Mg>Si); (b) slight enrichment of Al; (c) slight fluctuations of K, Ti and Fe; (d) strongly erratic enrichment and depletion of Mn; and (e) apparent increase of LOI. However, none of the elements show a regular trend of mobilization with depth.

Compared with their host CDG, particularly those immediately below and above the slip zones, concentrations of the major elements within the slip zones exhibit: (a) stronger depletions of Si and Mg, with maximum depletion within the slip zones along profiles at AP7 and TT2, and at AP7 and TT1A, respectively; (b) greater enrichment of Al and higher LOI, with greatest Al fixation within the slip zones along profiles at AP7 and TT2; (c) stronger enrichment of Fe, with the peak value within the slip zone along the profile at AP7; and (d) significant fixation of Mn along the three profiles (Fig. 5A–C). Furthermore, the degree of depletion or enrichments of these elements within the slip zones shows an order AP7<TT1A<TT2, in which the slip zones become increasingly more clayey (Fig. 5A–C). Distributions of other elements within the slip zones do not display consistent patterns along the profiles, and any significant differences from their host CDG (Fig. 5A–C).

Data from three pairs of sub-samples along the clay seam at SDZ (Fig. 6) reveals consistent variation patterns in concentrations of Mn, Fe, Na and LOI, with significant increase in Mn, slight increase in Fe and Na, and slightly lower LOI within DGS than those within WS. Concentrations of other elements within WS and DGS show irregular variations, and concentrations of each major element along DGS and WS are variable at different locations (Fig. 6).

Distributions of trace elements

Figure 7A–C display that distributions of the selected trace elements within the slip zones and their host CDG vary strikingly. With reference to the fresh granite, distribution of the trace elements along the profiles shows no consistent patterns with variable depletions and enrichments, except Sr which shows irregular depletion.

Compared with their host CDG, especially those immediately above and below the slip zones, ICP-MS results (Fig. 7A–C) reveal that within the slip zones there are stronger depletion of Sr and striking enrichment of Ba along the profiles. Similar to Mn variation within the slip zones along the three profiles, Ba concentrations also show an order of AP7<TT1A<TT2 (Fig. 7A–C). Distributions of other trace elements within the slip zones present no consistent patterns along the profiles (Fig. 7A–C).

Data from sub-samples along the clay seam at SDZ illustrates that there is a tendency of stronger fixations of Ba and Y, and slightly higher enrichment of Sc within DGS than within WS (Fig. 8). Again, concentrations of each trace element along DGS and WS are inconsistent at different locations.

Distributions of REE

Chondrite-normalized fresh granite (Fig. 9A–C) shows enrichments of light REE (LREE) relative to heavy REE (HREE) with a negative Eu-anomaly (Eu/Eu*=0.685) and flat HREE trend, similar to the typical REE patterns of some granitic rocks analyzed by Nesbitt (1979), Middelburg and others (1988), Aubert and others (2001), who attributed the negative Eu-anomaly to fractionation of plagioclase during formation of granite. Relative to the fresh granite, REE concentrations of all samples yield consistent trends of enrichment with stronger negative Eu-anomaly (Eu/Eu*=0.188–0.479) and significantly negative and positive Ce-anomalies, as well as slightly stronger enrichments of LREE relative to HREE (Fig 9A–C). Similar to major and trace elements, REE distributions show no regular trend with depth.

Strongest Eu-anomalies consistently occur within the slip zones compared with their host CDG (Fig 9A–C). Among

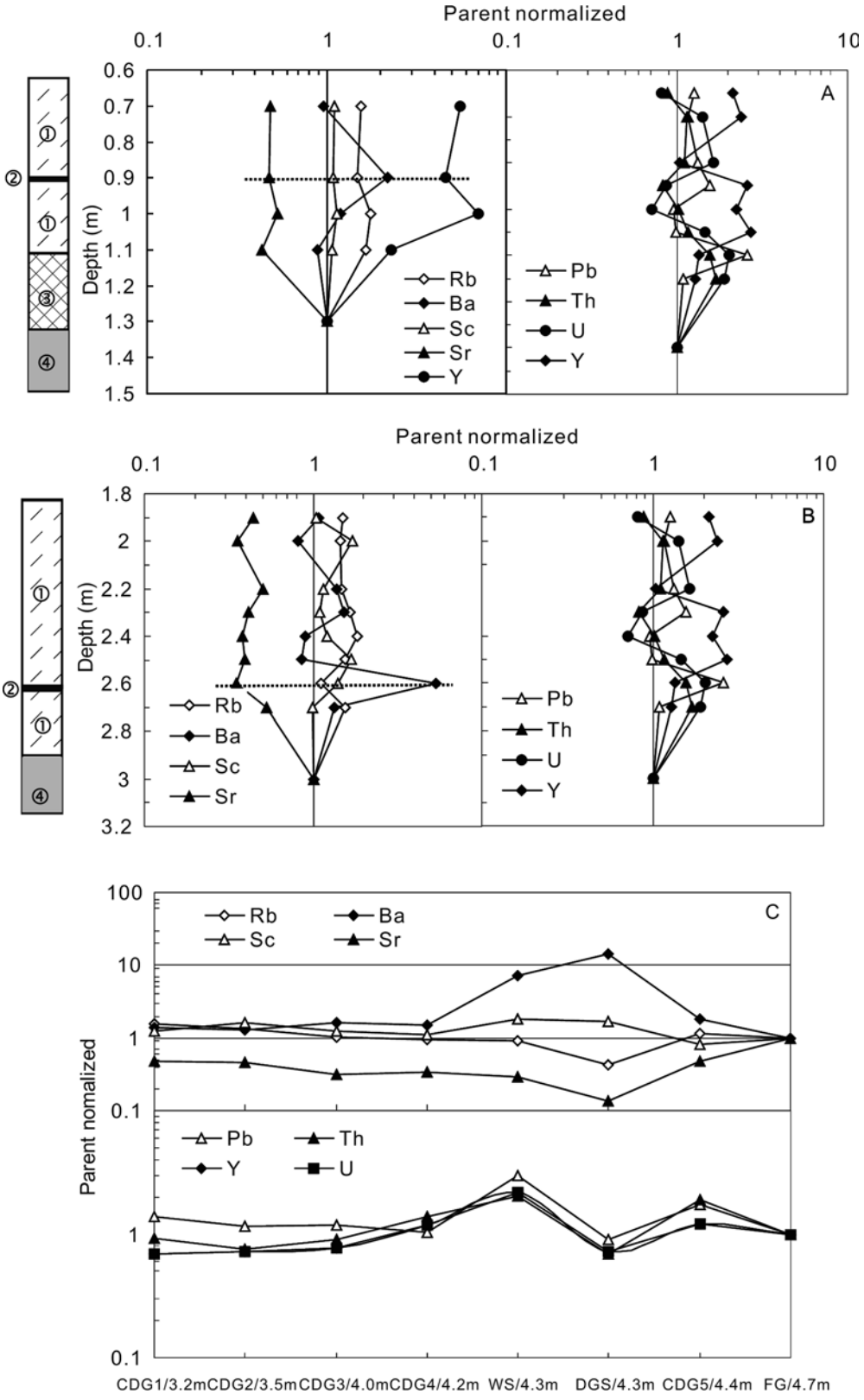

Fig. 7
Variations of trace element concentrations along profiles at AP7 (A), TT1A (B), TT2(C). (①-CDG; ②-Slip zone; ③-CDG-HDG; ④-Fresh rock.)

the slip zones along the three profiles, the order of Eu-anomalies is AP7 (Eu/Eu*=0.333) <TT1A (Eu/Eu*=0.291) <TT2 (Eu/Eu*=0.280). Notably, Ce-anomalies are positive within the slip zones, and negative within their host CDG (Fig. 9A–C). The magnitude of positive Ce-anomalies within the slip zones varies in the same order: AP7 (Ce/Ce*=1.162) <TT1A (Ce/Ce*=3.816) <TT2 (Ce/Ce*=8.470). Distributions of other REE of the slip zones are parallel to those of their host CDG, whereas their concentrations are lower than the CDG immediately below

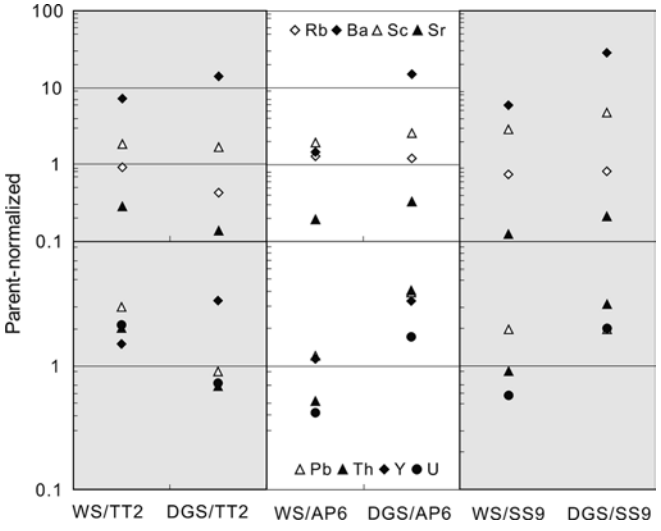

Fig. 8
Variations of trace element concentrations along the clay seam at SDZ

and above the slip zone at AP7, but lower than the overlying CDG and higher than the underlying CDG at TT1A and TT2 (Fig. 9A–C).

Data from the sub-samples along the clay seam at SDZ consistently show stronger positive Ce-anomaly, negative Eu-anomaly, and higher enrichment of other REE within DGS than those within WS (Fig. 10). REE concentrations along DGS and WS vary at different locations.

Occurrences of the prevailing major, trace and REE

EDS analyses (Fig. 11A–F) confirm the prevalence of major elements Si, Al, K, Mn and Fe, trace element Ba, and REE Ce within the slip zones. EDS results substantiate that Si, Al and K mainly occur as constituents of the primary minerals (quartz and K-feldspar) and secondary clay minerals, while Mn, Ba and Ce commonly co-exist as localized coating of fine matrix or relict primary minerals evidenced by their peaks coinciding with those of Al, Si and K (Fig. 11A–F). Generally, Ba and Ce only occur where Mn peak is the strongest among the elements detected (Fig. 11A–D). Locally, Mn, Ba and Ce are extremely concentrated, and the richest Ce occurs where Mn and Ba are less concentrated (Figs. 11E, F and 12A–C).

Discussion

Behaviors of chemical elements and their implications

Major elements

Variations of major elements within granitic saprolites strongly indicate the unstable nature of their primary minerals (plagioclase, biotite, K-feldspar and quartz), formation of secondary minerals, and mobility of each element in the course of weathering (Nesbitt 1979; Middelburg and others 1988; van der Weijden and van der Weijden 1995; Aubert and others 2001). Among the major elements analyzed within the granitic saprolite at this site: (a) greatest depletion of Ca and Na reflects intensive, and even complete decomposition of plagioclase and most mobile nature of these two elements; (b) weaker depletion of Mg could be related to the decomposition of biotite and its existence in octahedral crystal lattices of illite, as well as its affinity to Mn and Fe (Stevens and others 1979); (c) weaker depletion or slight enrichment of K can be attributed to slower decomposition of K-feldspar than plagioclase, and formation of illite (Duzgoren-Aydin and others 2002b); (d) slight variations of Fe and Ti may be explained by their less mobile nature than other elements and their occurrence in secondary oxides; and (e) depletion of Si, enrichment of Al and increase in LOI signify decomposition of primary minerals and formation of clay minerals, where good correlation between the Al to Si ratio and LOI (Fig. 13) confirms this relationship. Many studies (e.g., Middelburg and others 1988; Braun and others 1998; Vaniman and others 2002) showed that Mn with variable valence is a redox-sensitive element during weathering when highly mobile Mn (II) dissolved from natural minerals and rocks is easily oxidized into Mn (IV) and precipitated or adsorbed onto clays as insoluble Mn_2O, providing a direct indication of oxidation conditions. However, Mn oxidation and accumulation is a very complex dynamic process. Occurrence and intensity of Mn oxidation has been found to be largely related to solution chemistry (pH and Eh), and biological conditions, such as the presence of aerobic bacteria, while Mn accumulation is associated with intensity of oxidation and abundance of clays, rather than the parent rock (Crertar and others 1980; Middelburg and others 1988; Roy 1992; Krauskopf and Bird 1995; Braun and others 1998; Vaniman and others 2002).

Distribution of the major elements along the profiles (Fig. 5A–C) suggest that there must have been stronger intensity of primary mineral decomposition and greater abundance of secondary clay minerals, being in accordance with field, petrographic and XRD identification and particle size analysis (Table 1). Significant Mn accumulation within the slip zones indicate occurrence of active oxidation condition, and is also related to greater abundance of clays within the slip zones. Furthermore, the differences in the element concentrations among the slip zone segments correspond to increasing orders of decomposition of primary minerals and clay content: TT2>TT1A >AP7, again consistent with field, petrographic and XRD analyses (Table 1). Variations in Mn concentrations among the slip zone segments should be related mainly to clay content, and likely also to intensity of oxidation condition.

For DGS and WS within the clay seam at SDZ (Table 1 and Fig. 6): (a) slight differences in the concentrations of Si and Al coincide with little variation in their clay contents; (b) slightly lower LOI of DGS may be attributed to lower abundance of halloysite, a water-bearing clay mineral within its crystal structure (Wen 2002); and (c) slightly higher abundance of Na and Ca within DGS may be related to the presence of trace amounts of interstratified illite-smectite. Mn fixation indicates that oxidation conditions

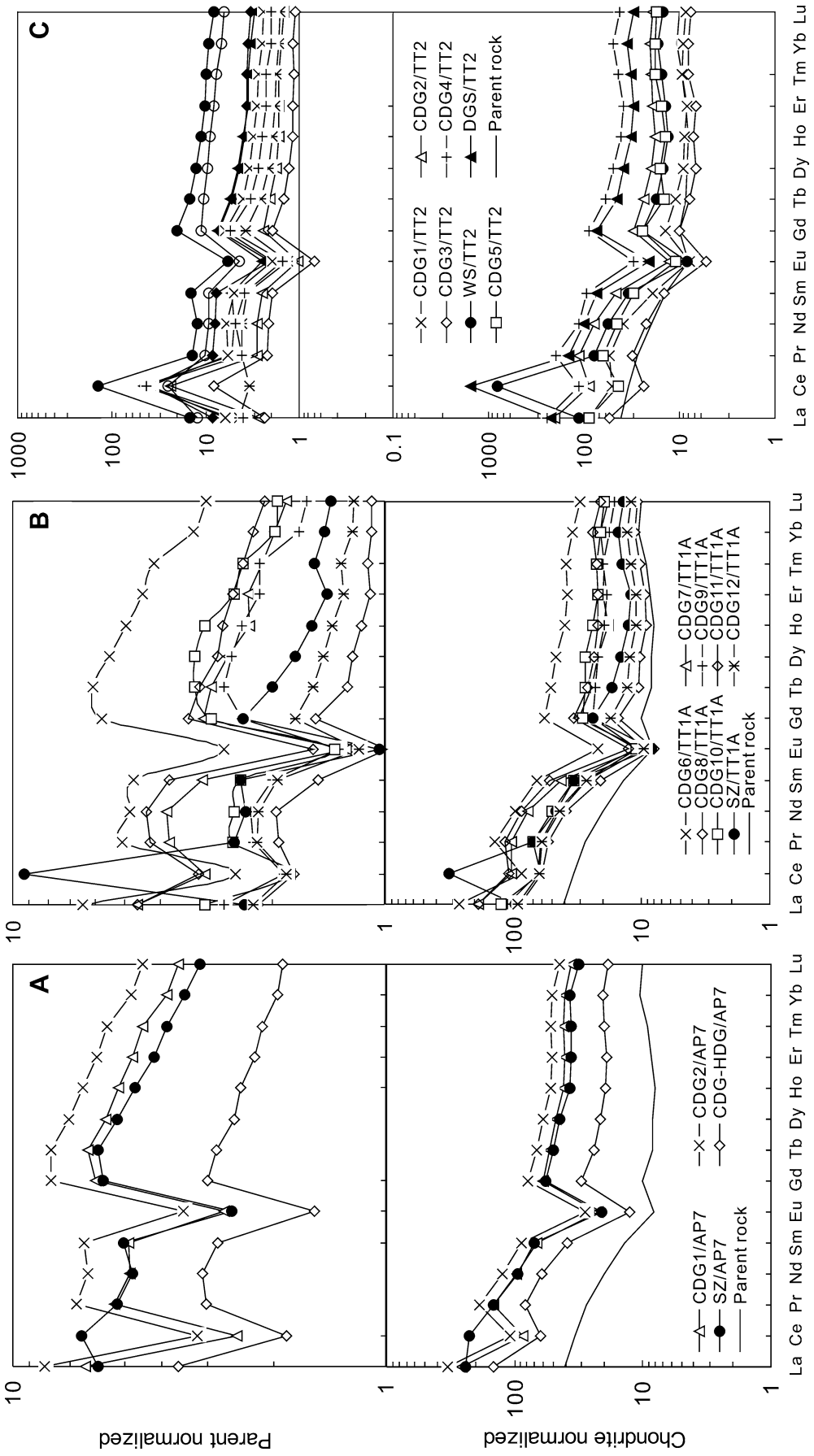

Fig. 9
Variations of REE concentrations along profiles at AP7 (A), TT1A (B), TT2(C)

must have occurred within DGS and WS. Interestingly, strikingly higher Mn concentration within DGS than within WS does not correlate with their clay contents: DGS has a lower clay content than WS at AP6 and SS9, implying that there must be other factors controlling Mn accumulation, in addition to clay abundance. DGS contains more kaolinite, but less halloysite than WS. It is thus believed that Mn concentration may also be associated with clay mineralogy. Variable concentrations of these elements at different locations along DGS and WS indicate that clay abundance and intensity of oxidation conditions are variable along these seams.

Variable distributions of the major elements with depth (Fig. 5A–C) suggest that downward leaching and deposition processes of the elements, either in the form of Al-Si solution or colloids, are not predominant. This could be due to superimposition of other forms of mobile behaviors of the elements, most likely lateral migration. Consequently, higher clay content of the clay seams at TT1A and TT2 than their host CDG may have resulted from: (a) downward leaching of Al and Si through pores and fissures, and deposition within the relict sheeting joints; and (b) lateral migration of Al and Si, and fixation within these joins. The clays within the slip zone at AP7, where it developed through CDG, may have also formed by these processes as a result of the high hydraulic connectivity of CDG. Both field and microscopic observations show that the contacts between the clay seam at TT2 and its host CDG are very rough (Fig. 4), indicating in-situ weathering of wall rocks of the relict sheeting joint. Therefore, WS, being in direct contact with the walls of the joint, is likely an in-situ weathering product of wall rocks with minor addition of transported Al-Si solution and colloidal particles. Correspondingly, DGS sandwiched by WS may have been formed mainly by transported Al-Si solution and colloidal clay particles within the joint with some minor mixing of in-situ weathering products. It is suspected that the clay deposition rate within the joint should be much slower than weathering of the wall rocks, resulting in very thin DGS and thick WS. Absence of WS within the clay seam at TT1A may be because local clay deposition rate within the joint is faster than in-situ weathering of the wall rocks (Fig. 6).

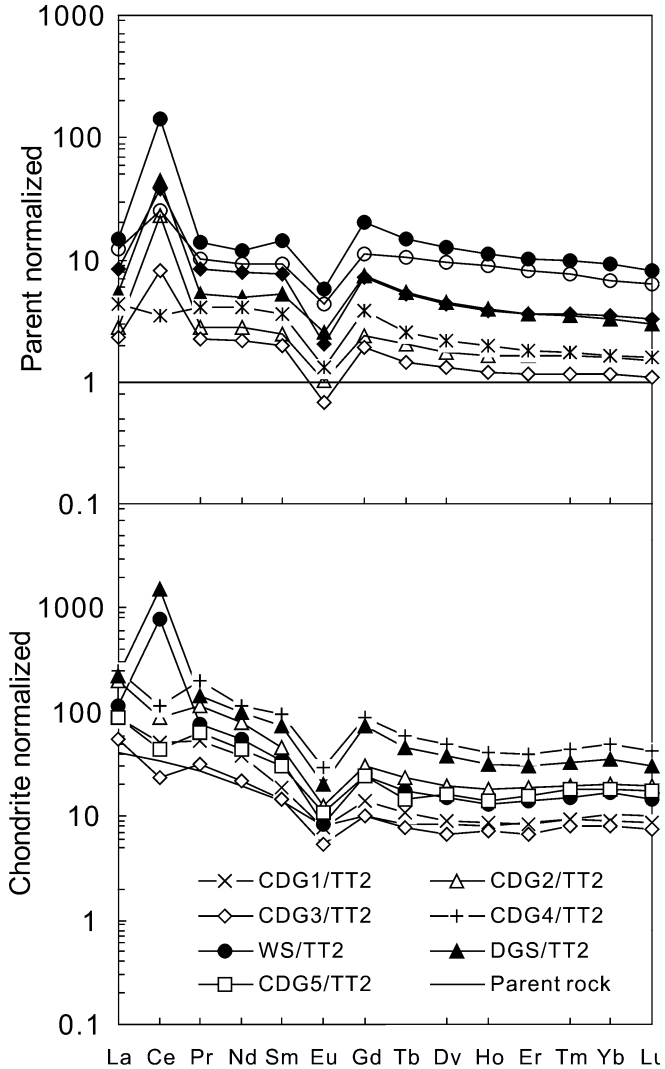

Fig. 10
Variations of REE concentrations along the clay seam at SDZ

Trace elements

Behaviors of trace elements are closely linked to the stability of the primary and accessory minerals in which they are present (Krauskopf and Bird 1995; Dequincey and others 2002). Trace elements are also found to be readily absorbed onto clay size particles (Middelburg and others 1988; Vaniman 2002). Thus, trace elements display complex behaviors during weathering. Depletion of Sr within the slip zones and their host materials at the study site may be related to decomposition of plagioclase in which Sr occurs as a substitute for Ca, which supports stronger plagioclase decomposition within the slip zones. Many workers, e.g., Middelburg and others (1988), Braun and others (1998), Palumbo and others (2001), and Vaniman and others (2002), demonstrated that Ba is easily scavenged by Mn, showing high affinity for Mn in diverse redox-active environments. Significant fixation of Ba within the slip zones (Fig. 5A–C) is thus most likely associated with Mn, giving an indirect clue for active oxidation microenvironment within the slip zones relative to their host materials. Corresponding to Mn occurrence, Ba accumulation among the slip zone segments (Figs. 7A–C, and 8) may also be associated with both abundance and mineralogy of clay (Table 1).

REE

The REE are primarily found in trivalent oxidation state, and have almost identical chemistry, except Eu and Ce. It has been well documented that REE can be fractionated and leached during advanced weathering, showing that

►

Fig. 11
Backscattered SEM images of the slip zone at TT2 (A), AP6 (C) and TT5U (E), and X-ray spectra patterns of clay coated with Mn, Ba and Ce on the point indicated on image A (B), C (D) and E (F)

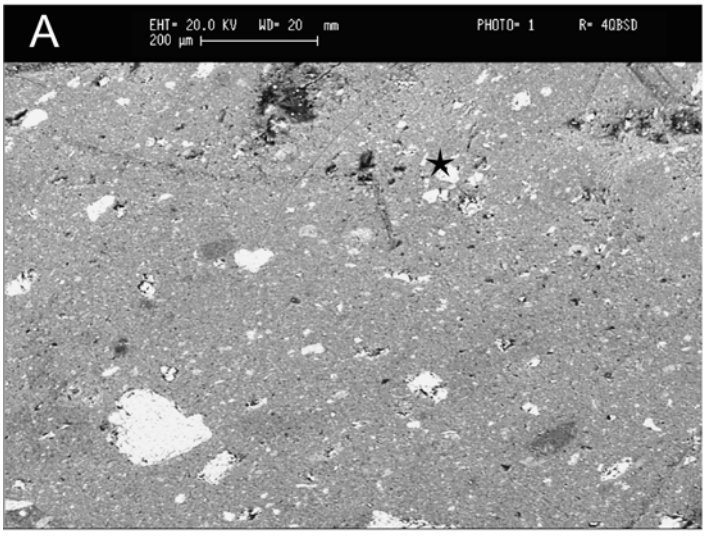
A
EHT= 20.0 KV WD= 20 mm
200 µm
PHOTO= 1 R= 4QBSD

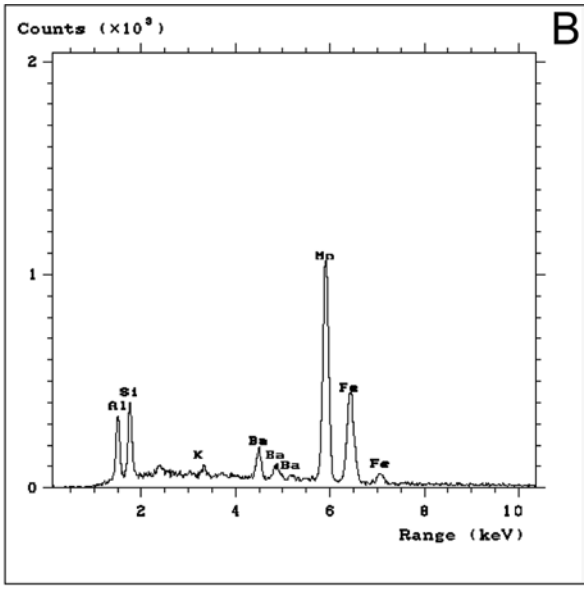
B
Counts (×10³)
Mn
Fe
Si
Al
K
Ba
Ba
Ba
Fe
Range (keV)

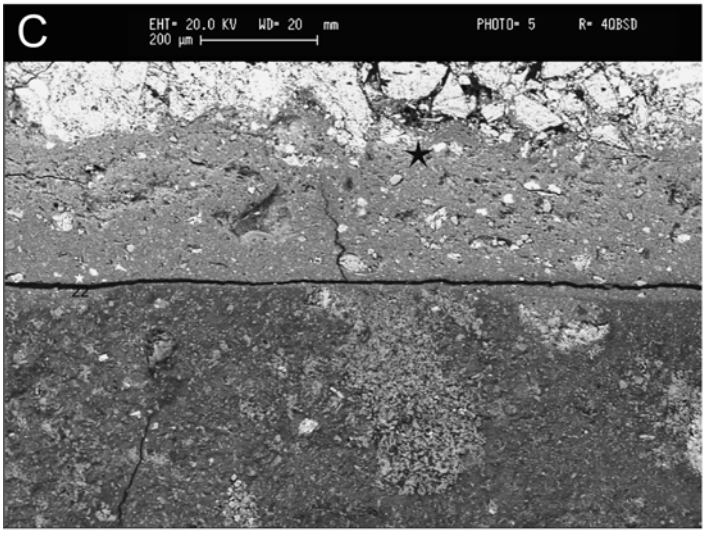
C
EHT= 20.0 KV WD= 20 mm
200 µm
PHOTO= 5 R= 4QBSD

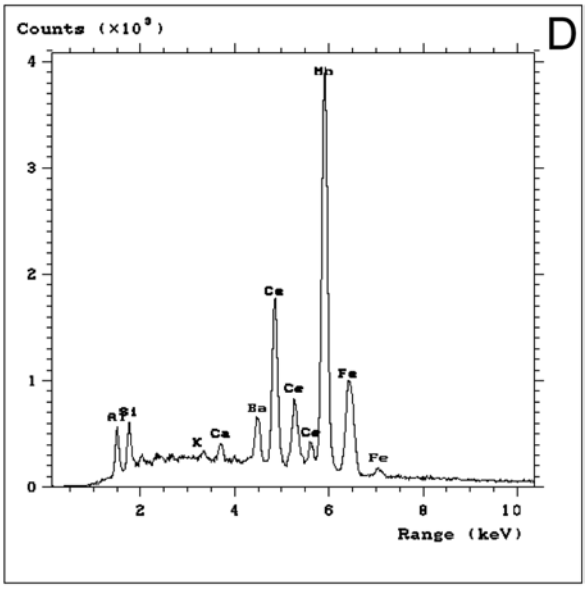
D
Counts (×10³)
Mn
Ce
Ce
Ce
Fe
Ba
Si
Ca
K
Fe
Range (keV)

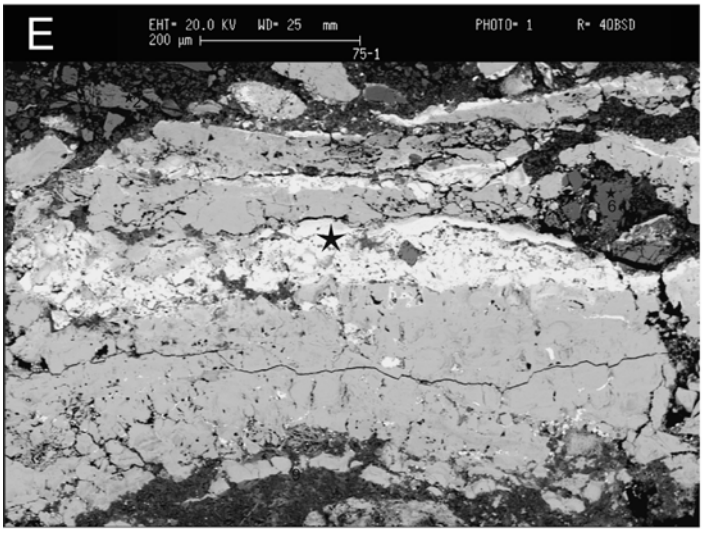
E
EHT= 20.0 KV WD= 25 mm
200 µm
PHOTO= 1 R= 4QBSD
75-1

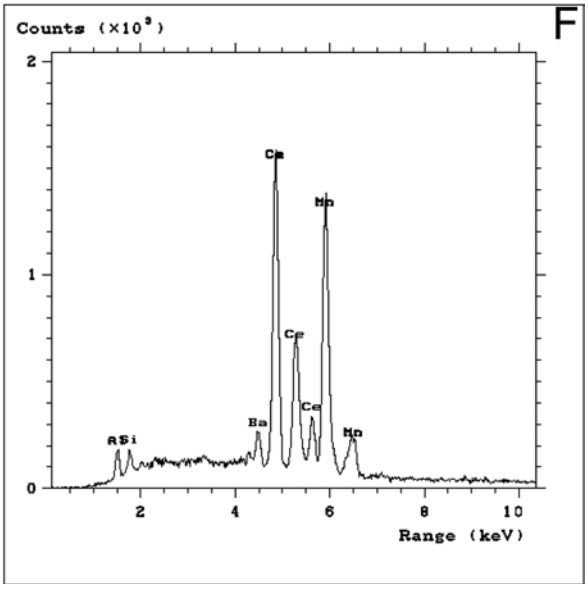
F
Counts (×10³)
Ce
Mn
Ce
Ce
Ba
Si
Mn
Range (keV)

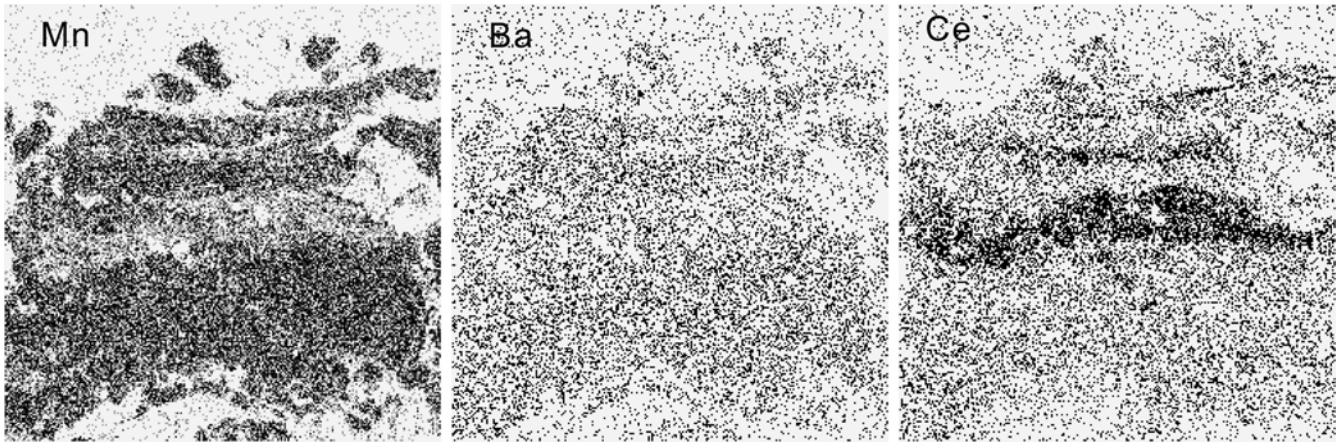

Fig. 12
X-ray element maps on the image in Fig. 11E

most REE are fixated with stronger enrichments of LREE relative to HREE (Nesbitt 1979; Middelburg and others 1988; Braun and others 1990, 1998; van der Weijden and van der Weijden 1995; Koppi and others 1996; Aubert and others 2001; Vaniman and others 2002). The REE behaviors suggest their low mobility, and relatively stronger mobility of HREE than LREE. Eu (II), occurring in granite as a substitute for Ca within plagioclase, is highly soluble and much more easily leached than the trivalent REE, while Ce (III), present in primary and accessory minerals, is readily converted into Ce (IV), and enriched as immobile CeO_2 under oxidation condition, behaving very similar to Mn as a redox-sensitive element. Chemical behaviors of REE during weathering depend on several factors: Eh, pH, presence of organic and inorganic ligands (Cantrell and Byrne 1987), clay abundance (Aagard 1974), and parent rock mineralogy.

Evidently, relative to the parent rock, REE patterns of the granitic saprolite at this site (Fig. 9A–C) suggest occurrence of intense decomposition of plagioclase and active oxidation conditions. Compared with their host materials, stronger negative Eu-anomalies within the slip zones (Fig. 9A–C) reflect more intense Eu fractionation as a result of stronger decomposition of plagioclase, marked by their greater Eu/Eu* anomalies, and evidenced by little or no plagioclase from microscopic observations, and

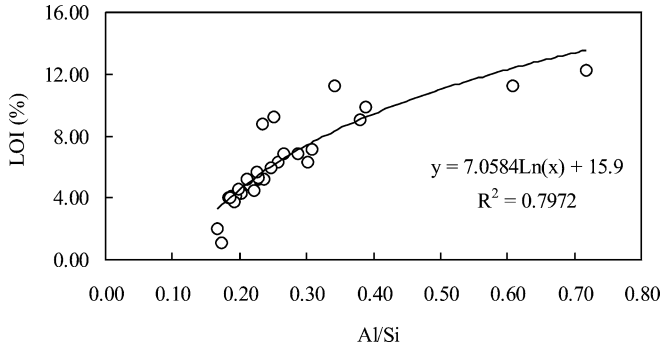

Fig. 13
Correlation of Al/Si ratio and LOI within the granitic saprolite

consistent with the indication from Sr distribution. Similarly, significant positive Ce-anomalies within the slip zones indicate pronounced oxidation processes, consistent with the possibility implied by Mn behavior. Although REE behaviors are influenced by several factors as aforesaid, it is suspected that parallel REE patterns of the slip zones and their host materials may be also associated with variations of drainage conditions in different horizons, as percolating water or influx is obviously one of the most important media removing or transporting REE. Thus, concentration differences of other REE may imply a contrast in drainage conditions between the slip zones and their immediately host materials, consistent with their physical nature. However, this relationship needs to be further investigated, and actual behaviors of REE within the slip zones and their host materials should be linked with influences of all the factors. Along the slip zone segments (Fig. 9A–C): (a) differences in negative Eu-anomalies indicate an increasing intensity of plagioclase decomposition, AP7<TT1A<TT2; (b) differences in positive Ce-anomalies may be largely attributed to their different clay contents, as for Mn and Ba; and (c) concentration differences of other REE may also related to different drainage conditions. Variations of REE concentrations between DGS and WS within the clay seam at SDZ also suggest: (a) stronger decomposition of plagioclase within DGS marked by higher negative Eu anomalies; (b) likely clay mineralogic influence on positive Ce anomalies; and (c) possibly a contrast in drainage conditions implied by concentration difference of other REE. Additionally, variations in REE concentrations among different segments of DGS and WS of the clay seam at SDZ (Fig. 10) could also be attributed to non-uniform intensity of plagioclase decomposition, abundance and mineralogy of clay, as well as drainage conditions.

Mn, Ba and Ce associations and their implications

Mn oxide has high sorption capacity for heavy metals in soils (Koppi and others 1996; Palumbo and others 2001). EDS analyses confirm that Ba and Ce commonly coexist with Mn within the slip zones. Concurrence of Mn, Ba and Ce (Fig. 11A–F) suggests Ba and Ce have the highest affinity for Mn than other heavy metals, similar to those illustrated by Fleet (1984), Middelburg and others (1988), Koppi and

others (1996), Braun and others (1998), Palumbo and others (2001), and Vaniman and others (2002). Good correlations among the concentrations of Mn, Ba and Ce from bulk samples (R^2=0.91–0.96) statistically substantiate their close associations (Fig. 14). In addition, active redox further mediates association between Mn and Ce . However, EDS results and statistical analyses show that Ba has higher affinity for Mn than Ce (Figs. 11A–F and 14). Local separation of Mn and Ce (Figs. 11E, F, 12A–C) indicates these two elements also have different behaviors during evolution of the slip zones. Associations and distinctions of Mn, Ba and Ce behaviors suggest that at least two kinds of microenvironments existed within the slip zones.

Prevailing oxidation conditions

Striking accumulations of Mn, Ba and Ce within the slip zones and their close associations provide strong indication that oxidation conditions prevailed during their formation and evolution. As mentioned earlier, oxidations of Mn and Ce are controlled by several factors: pH, Eh, biological conditions, clay abundance and clay mineralogy, and their accumulations follow a very complex dynamic course. Krauskopf and Bird (1995) and Braun and others (1998) showed that oxidation of Mn (II) could occur either when it is exposed to air or dissolved in oxygenated water. Subsurface occurrence of the slip zones of the landslide indicates that Mn oxidation could only occur when there is a supply of oxygenated water in an open system through the process (Krauskopf and Bird 1995; Braun and others 1998):

$$Mn^{2+} + 2H_2O \rightarrow MnO_2 + 4H^+ \quad (1)$$

when Eh ranges between 0.15 to 1.15 V and regardless of pH. At the study site, such oxygenated water can only be provided by rainwater through the infiltration process. As described previously, rainfall infiltration was the predominant hydrodynamic process within the upper groundwater regime in which the slip zones were located, hence greatly facilitating Mn oxidation process. Similarly, upon weathering in an open system with oxygenated water, soluble and mobile Ce (III) is oxidized into immobile CeO_2 through the equilibrium process (Braun and others 1990, 1998):

$$Ce^{3+} + 2H_2O \rightarrow CeO_2 + 4H^+ \quad (2)$$

when pH ranges from 2.5 to 7.5 and Eh from −0.4 to 1.1 V (Braun and others 1990). Consequently, coexistence of Mn and Ce as a result of co-precipitation or adsorption onto clays is observed if conditions favor the formation of MnO_2 and CeO_2. Simultaneously, Ba is scavenged accompanying precipitation of Mn_2O (Krauskopf and Bird 1995). Except sufficient supply of oxygenated water, accumulation of Mn, Ba, and Ce oxides should also require a very slow rate of water flow, i.e., a poor drainage condition, enabling generation of oversaturated oxides within the fluid, and allowing these oxides to precipitate or to be absorbed onto clays. Hence, distribution of Mn, Ba and Ce may indicate that there is a contrast in drainage conditions between the slip zones and their host materials, similar to their REE behaviors as discussed previously. However, as behaviors of Mn and Ce also depend on hydrochemistry (pH, Eh), biologic environment and clay abundance, their concentrations may not directly indicate the nature of drainage conditions. Correspondingly, weak enrichments or depletions of Mn, Ba and Ce (and other REE) within the host materials of the slip zones may be largely attributed to strong leaching conditions, under which dissolved Mn, Ba, and Ce are washed away so rapidly that they do not have sufficient time for any reaction, e.g., oxidation by oxygenated rainwater, although oxidation conditions are still active there. As mentioned earlier, there are higher abundance of kaolinite and lower halloysite within DGS of the clay seam at SDZ than WS (Table 1). Keller (1970) and Mitchell (1993) showed that kaolinite is generally favored where drainage and precipitation cooperates, whereas halloysite often forms under well-drained and exceptionally strong leaching conditions. Hence, in terms of hydrodynamics, kaolinite and halloysite occur under slow and fast water flow conditions, respectively. This explains why much greater concentrations of Mn, Ba and Ce took place within DGS than those within WS.

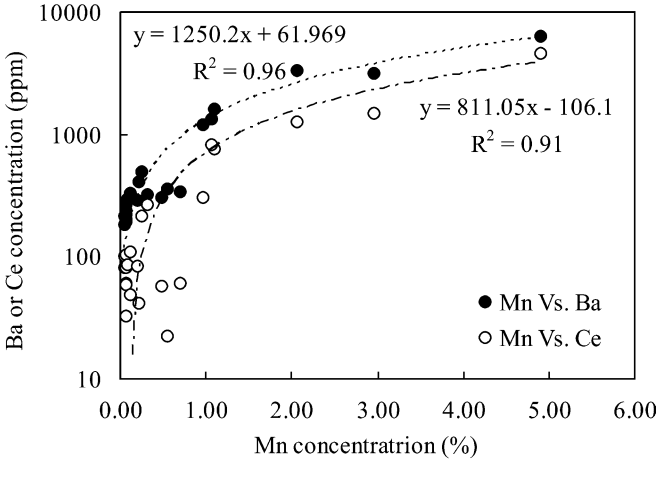

Fig. 14
Correlations of Mn with Ba and Ce within the slip zones and their host materials

Localized reduction conditions

Local separation of Mn and Ce, showing that the strongest concentration of Ce occurs where concentration of Mn is much weaker (Figs. 11E, F, and 12A–C), suggests that there may be a local reduction condition under which Mn (IV) reduces to mobile Mn (II), resulting in relatively stronger Ce enrichment and weaker Mn accumulation. Koppi and others (1996) explained that separation of Mn and Ce probably results from reduction of MnO_2 to MnOOH when the following reaction proceeds from right to left:

$$MnOOH + 1/4O_2 = MnO_2 + 1/2H_2O \quad (3)$$

subsequently:

$$Ce^{3+} + MnOOH = CeO_2 + Mn^{2+} + H^+ \quad (4)$$

MnO_2 is normally immobile under natural conditions with little solubility (Krauskopf and Bird 1995; and Braun and

others 1998). However, Mn (IV) could reduce to the mobile Mn (II) when certain microbial species, particularly some anaerobic bacteria or organic acids, are active within soil (Crertar and others 1980; Roy 1992). Due to its very poor solubility, reduction of Mn (IV) should have proceeded very slowly. In this case, hydrodynamically, rate of water flow should also be very slow. The reaction on the right-hand-side of Eq. (3) may have been first initiated by microbial catalysis, which facilitates to scavenge the oxygen on the left-hand-side and to advance the reaction to the right-hand-side, resulting in continuous release of O_2 on the right hand side. Subsequently, newly produced Mn^{2+} in Eq. (4) may have been removed by percolating water, leaving CeO_2 behind.

The existence of Mn and Ba within the richest Ce zone, as shown in Fig. 11A–C, may be due to: (a) the remnant MnO_2, which was not fully dissolved during the subsequent Mn reduction and abnormal Ce enrichment; and/or (b) newly formed MnO_2 following abnormal Ce fixation. This suggests that at least two phases of redox cycles have occurred within Ce rich zone.

Conclusions

This comprehensive study on geochemical characteristics of the slip zones of the landslide in a granitic saprolite substantiates that the slip zones of landslides developed along pre-existing weak zones do have distinct geochemical nature from their host materials, similar to their physical and mechanical nature.

In this study, results from three profiles across the slip zones at different locations consistently show that there are stronger depletion of Si, higher enrichment of Al, greater LOI and significant fixations of Mn, Ba and Ce within the slip zones compared with their host materials, as well as stronger negative Eu anomalies and higher enrichments of other REE. The ratio of Al to Si is closely correlated with LOI. Occurrences and concentrations of Ba and Ce are generally intimately associated with Mn, showing their high affinities for Mn. Locally, separation of Mn and Ce is observed.

Distinct geochemical characteristics of the slip zones provide strong clues for the formation and microenvironments of the slip zones. Distribution of Al, Si and LOI suggest that: (a) there are greater abundance of clays within the slip zones, consistent with field and microscopic observations; (b) the formation of clays within the slip zones is probably by downward leaching and deposition of Al-Si, and lateral migration of Al-Si through pores and fractures within the saprolite, in the forms of Al-Si solution and colloids. Existence of relict sheeting joints provides preferential pathways not only for element migration and deposition, but also for intensive weathering. The clay seams of the slip zones were thus developed along one or more sheeting joints. DGS of the clay seam at SDZ of the landslide may largely consists of clays from transported Al-Si solution and colloids, while WS may be likely the product of intensive in-situ weathering of the walls of the joint. Close associations of Mn, Ba and Ce, and REE patterns within the slip zones consistently imply that there were prevailing active oxidation and poorer drainage conditions, while local separation of Mn and Ce indicates that occasional reduction conditions may have also existed.

This study shows that geochemistry could be a useful tool to gather information for understanding the origin of slip zones and their microenvironments in landslide investigations, which is of great significance for delineating and predicting landslides.

Acknowledgements The work described in this paper was partially supported by a grant from the Research Grants Council of the Hong Kong Special Administrative Region, China (Project No. HKU 7002/03P). The authors acknowledge kind assistance provided by Mr. Liang Qi and the supporting staff of the Department of Earth Sciences and Electron Microscopy Unit of the University of Hong Kong in carrying out XRF, ICP-MS and EDS analyses.

Appendix: List of Abbreviations

Material weathering grades within the host granitic saprolite:

CDG: Completely Decomposed Granite (Weathering Grade of V)
HDG: Highly Decomposed Granite (Weathering Grade of IV)
MDG: Moderately Decomposed Granite (Weathering Grade of III)
SDG: Slightly Decomposed Granite (Weathering Grade of IV)

Field-scale deformational divisions of the investigated landslide:

NDZ: Northern Distressed Zone
SDZ: Southern Distressed Zone

Seams differentiated within SDZ:

DGS: Dark Gray Seam (Slip Zone)
WS: White Clay Seam(s)

Exploratory excavations:

AP: Trial Pit
TT: Trial Trench
SS: Surface Strip

Techniques:

XRF: X-Ray Fluorescence Spectrometry
SEM: Scanning Electron Microscopy
ICP-MS: Inductively Coupled Plasma-Mass Spectrometry
EDS: Energy Dispersive X-Ray Spectrometry

Chemical elements/indices:

LOI: Loss on Ignition
REE: Rare Earth Element(s)
LREE: Light REE
HREE: Heavy REE

References

Aagard P (1974) Rare earth elements adsorption on clay minerals. Bull Group Franc Argiles 26:193–199

Anson RWW, Hawkins, AB (1999) Analysis of a sample containing a shear surface from a recent landslide, south Catswolds, UK. Geotechnique 49:33–41

Aubert A, Stille P, Probst A (2001) REE fractionation during granite weathering and removal by waters and suspended loads: Sr and Nd isotopic evidence. Geochim Cosmochim Acta 65(3):387–406

Brand EW (1995) Slope stability and landslides under tropical conditions—a review. Proc Symp Hillside Development, Kuala Lumpur, Malaysia

Braun J-J, Pagel M, Muller J-P, Bilong P, Michard A, Guillet B (1990) Cerium anomalies in lateritic profiles. Geochim Cosmochim Acta 54:781–795

Braun J-J, Viers J, Dupre B, Polve M, Ndam J, Muller J-P (1998) Solid/liquid REE fractionation in the lateritic system of Goyoum, East Cameroon: the implication for the present dynamics of the soil covers of humid tropical regions. Geochim Cosmochim Acta 62(2):273–299

Cantrell KJ, Byrne RH (1987) Rare earth elements complexation by carbonate and oxalate ions. Geochim Cosmochim Acta 51:597–605

Crertar DA, Fischer AG, Plaza CL (1980) Metallogenium and biogenic deposition of manganese from Precambrian to Recent time. In: Varentsov IM, Grasselly G (eds) Geology and geochemistry of manganese. Stuttgart, Schweizerbart's Sche, vol 3, pp 285–303

Cruden DM, Varnes DJ (1996) Landslide types and processes. In: Turner AK, Shuster RL (eds) Landslides investigation and mitigation. Transportation Research Board, US National Research Council, Washington, DC, Spec Rep No 247, pp 36–75

Dequincey O, Chabaux F, Clauer N, Sigmarsson O, Liewig N, Leprun J-C (2002) Chemical mobilization in laterite: evidence from trace elements and 238U-234U-230 Th disequilibria. Geochim Cosmochim Acta 66(7):1197–1210

Dikau R, Brunsden D, Schrott L, Isen M-L (1996) Landslide recognition, identification, movement and courses. Report of 1st of the European Commission Environment Programme. Wiley, New York

Duzgoren-Aydin NS, Aydin A, Malpas J (2002a) Re-assessment of chemical weathering indices: case study from pyroclastic rocks of Hong Kong. Eng Geol 63:99–119

Duzgoren-Aydin NS, Aydin A, Malpas J (2002b) Distribution of clay minerals along a weathered pyroclastic rock profile. Catena 50:17–41

Fleet AJ (1984) Aqueous and sedimentary geochemistry of the rare earth elements. In: Henderson P (ed) Rare earth element geochemistry. Elsevier, Amsterdam, pp 343–373

Fletcher CJN, Campbell SDG, Carruthers RM, Busby JP, Lai KW (1997) Regional tectonic setting of Hong Kong: implication of new gravity models. J Geol Soc Lond 154:1021–1030

FMSW (Fugro Maunsell Scott Wilson Joint Venture) (2000) Report on the Shek Kip Mei landslide of 25 August 1999, vol 1

Hürlimann M, Ledesman A, Marti J (2001) Characterization of a volcanic residual soil and its implication for large landslide phenomena: application to Tenerife, Canary Islands. Eng Geol 59:115–132

Hutchinson JN (1988) General report morphological and geological parameters of landslides in relation to geology and hydrogeology. In: Bonnard C (ed) Proc 5th Int Symp on Landslides. AA Balkema, Rotterdam, vol 1, pp 3–36

Keller WD (1970) Environmental aspects of clay minerals. J Sediment Petrol 40:788–813

Kenny TC (1977) Residual strength of mineral mixtures. Proc 9th Int Conf on Soil Mechanics and Foundation Engineering, Tokyo, vol 1, pp 155–160

Koor NP, Parry S, Yin J-H (2000) The shear strength of infilled and slicksided discontinuities of some Hong Kong saprolites. Eng Geol HK 2000, pp 187–192

Koppi AJ, Edis R, Field DJ, Geering HG, Klessa DA, Cockayne DJH (1996) Rare earth element trend and cerium-uranium-manganese associations in weathered rock from Koongarra, Northern Territory, Australia. Geochim Cosmochim Acta 60(10):1695–1707

Krauskopf KB, Bird D (1995) Introduction to geochemistry. McGraw-Hill, New York

Mashana NS, Suzuki A, Kitazono Y (1993) Effects of weathering on stability on natural slopes in north-central Komamoto. Soils and foundations 33(4):74–87

Middelburg J-J, van-der-Weijden C-H, Woittiez J-R (1988) Chemical processes affecting the mobility of major, minor and trace elements during weathering of granitic rocks. Chem Geol 68(3–4):253–273

Mitchell JK (1993) Fundamentals of soil behavior, 2nd edn. Wiley, New York

Nesbitt HW (1979) Mobility and fractionation of rare earth elements during weathering of a granodiorite. Nature 279:206–210

Palumbo B, Bellanca A, Neri R, Roe MJ (2001) Trace metal partitioning in Fe-Mn nodules from Sicilian soils, Italy. Chem Geol 173:257–269

Roy S (1992) Environments and processes of manganese deposits. Econ Geol 87:1218–1236

Shuzui H (2001) Process of slip surface development and formation of slip surface clay in landslide in Tertiary volcanic rocks, Japan. Eng Geol 61:199–219

Skempton AW, Petley DJ (1967) The strength along structural discontinuities in stiff clays. Proc Geotechnical Conf. Oslo, vol 2, pp 29-46

Stevens MB, Glasson MJ, Keays RR (1979) Structural and chemical aspects of metamorphic layering development in matasediments from Clunes, Australia. Am J Sci 279:129–160

van der Weijden CH, van der Weijden RD (1995) Mobility of major, minor and some redox-sensitive trace elements and rare-earth elements during weathering of four granitoids in central Portugal. Chem Geol 125:149–167

Vaniman DT, Chipera SJ, Bish DL, Duff MC, Hunter DB (2002) Crystal chemistry of clay-Mn oxide associations in soils, fractures, and matrix of the Bandelier Tuff, Pajarito Mesa, New Mexico. Geochim Cosmochim Acta 66(8):1349–1374

Wen BP (2002) Nature and development of slip zones of landslides in igneous saprolites, Hong Kong. PhD Thesis, The University of Hong Kong

Wen BP, Aydin A (2003) Microstructural study of a natural slip zone: quantification and deformation history. Eng Geol 68:289–317

Wen BP, Aydin A (2004) Deformation history of a landslide slip zone in light of soil microstructure. Environ Eng Geosci 10(2):123–150

Zheng G, Lang Y, Takano B, Matsuo M, Kuno A, Tsushima H (2002) Iron speciation of sliding mud in Toyama Prefecture, Japan. J Asian Earth Sci 20:955–963